### **Research Article**

**DE GRUYTER** 

Mei-Ling Zhuang, Li Gao\*, Fangzhi Zhu, Chuanzhi Sun\*, Hanbo Zhu, Changrong Yu, and Yan Qiao

# Flexural performance of a new type of slightly curved arc HRB400 steel bars reinforced one-way concrete slabs

https://doi.org/10.1515/rams-2023-0130 received May 13, 2023; accepted September 24, 2023

Abstract: In the present study, a new type of slightly curved arc HRB400 steel bars (SCAHSs) was proposed to solve the problem of temperature-induced stress loss in mass concrete structures without cutting off steel bars. The flexural performance of SCAHSs and straight HRB400 steel bars reinforced one-way concrete slabs were first experimentally investigated. Then, the effects of the shape and dimension of SCAHSs on the distribution and width of concrete cracks were analyzed and discussed. Subsequently, the synergistic tensile work characteristics between SCAHSs and concrete were presented. Finally, equations for the bearing capacity and allowable crack widths for SCAHSs in hydraulic massive structures were proposed. The test results indicated that after replacing the straight steel bars in the concrete slab with SCAHSs, the crack width of the concrete slabs increased, with the maximum crack width at the bottom of the concrete slabs increasing by a factor of 1.2–1.4. As the rise-span ratio of SCAHSs increased, the flexural stiffness of SCAHSs reinforced concrete slab decreased slightly, but the deflection increased. The allowable crack widths of SCAHSs reinforced concrete

**Keywords:** reinforced concrete slabs, flexural performance, allowable crack widths

### 1 Introduction

Mass concrete structures are common in hydraulic and hydropower projects. During construction, the temperature stress in mass concrete is relatively large. At the same time, mass concrete structures are susceptible to large temperature stresses due to the influence of external ambient temperature [1,2], leading to thermal cracks in concrete structures [3]. Therefore, wide slots are set to cast the mass concrete into blocks. The wide slots are backfilled in the later low-temperature season to form a whole. This measure has been proven to be effective in reducing and avoiding temperature cracks and is widely used in engineering [4].

There is usually steel bar passing through the wide slots. As the heat of hydration of the concrete decreases, both the concrete and the straight steel bars on both sides of the wide slot shrink. Due to the confining effect [5,6], the reinforcement will generate higher tensile stresses during construction [7], which reduces the load-bearing of the reinforcement during construction [8]. Lateral concrete also generates tensile stress and is more prone to cracking during construction [9,10]. It is common practice to cut the reinforcement across the wide slot within 24-48 h after the concrete is poured on both sides of the wide slot, and then connect it as a whole when the wide slot is backfilled later in the cold season. Typically, extruded sleeve connections and welded connections are used to connect the reinforcement. Currently, there are three ways to pass the reinforcement through wide slots, such as uncut reinforcement, cut reinforcement followed by extruded sleeve connection, and cut reinforcement followed by welded connection [11]. However, it is difficult to maneuver reinforcement through

Mei-Ling Zhuang, Changrong Yu: School of Transportation and Civil Engineering, Nantong University, Nantong, 226019, China Fangzhi Zhu, Hanbo Zhu, Yan Qiao: School of Civil Engineering and Architecture, Suqian College, Suqian, 223800, China; Jiangsu Province Engineering Research Center of Prefabricated Building and Intelligent Construction, Suqian College, Suqian, 223800, China

slabs under environment categories I, II, and III were 0.20, 0.17, and 0.12 mm, respectively.

<sup>\*</sup> Corresponding author: Li Gao, School of Civil Engineering and Architecture, Suqian College, Suqian, 223800, China; Jiangsu Province Engineering Research Center of Prefabricated Building and Intelligent Construction, Suqian College, Suqian, 223800, China, e-mail: gaoli@squ.edu.cn

<sup>\*</sup> Corresponding author: Chuanzhi Sun, School of Civil Engineering and Architecture, Suqian College, Suqian, 223800, China; Jiangsu Province Engineering Research Center of Prefabricated Building and Intelligent Construction, Suqian College, Suqian, 223800, China, e-mail: schzh\_xzh@163.com

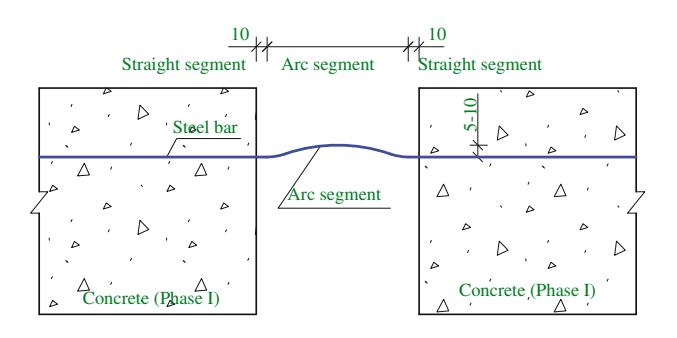


Figure 1: Diagram of SCASB across wide slot (unit: cm).

wide slots using pre-cut and post connections. It is almost impossible to implement when there are many layers of reinforcement crossing a wide slot. Therefore, how to handle reinforcement through wide slots is an urgent challenge in construction. Figure 1 shows a slightly curved arc steel bar (SCASB) without cutting off across a wide slot [12]. The SCASB across wide slot is used to accommodate the temperature deformation of the concrete on both sides of the wide slot by using the expansion and contraction of its slightly curved arc section. Due to the existence of the slightly curved arc section, its axial stiffness is less than that of the straight steel bar thus reducing the restriction on the temperature deformation of the concrete on both sides of the wide slot. But in the slightly curved arc section, stress concentration occurs at the top of the arc and at the backbend point of the SCASB, which is prone to enter into a plastic state.

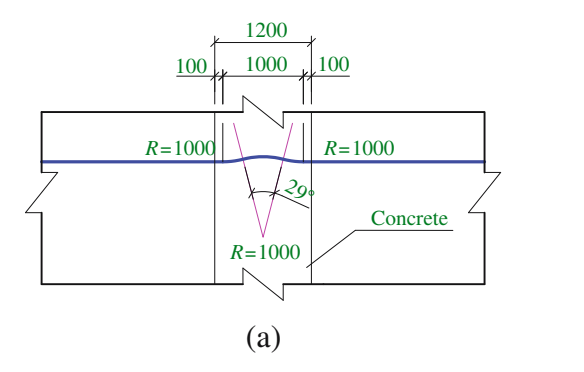
Currently, there is no knowledge on the flexural performance of the SCASBs reinforced with concrete slabs. To promote the application of SCASBs in hydraulic and hydropower structures, the flexural performance of a new type of slightly curved arc HRB400 steel bars (SCAHSs) reinforced one-way concrete slabs was investigated. Three sets of SCAHSs reinforced concrete slab specimens and one set of straight HRB400 steel bars reinforced concrete

slab specimens were first designed and fabricated. Then, the damage process of the specimens was observed through the flexural tests of the slabs. The crack expansion pattern and damage mechanism of the slabs were analyzed. The effects of the shape and dimension of SCAHSs on the distribution and width of concrete cracks were analyzed and discussed. Later, the synergistic tensile work characteristics between SCAHS and concrete were classified. Finally, equations for calculating the bearing capacity and the allowable crack width of SCAHSs in hydraulic massive structures were presented.

### 2 Experimental design and loading

### 2.1 Design and fabrication of reinforced concrete slab specimens

The design details of the two types of SCAHSs across a wide slot are shown in Figure 2. The form of the SCAHSs was 1 big arc + 2 small arc + 2 horizontal sections. The horizontal section length of SCAHSs was 100 mm. The radiuses of their arcs were different. For type I, the wide slot width of SCAHSs was 1.5 m. For Type II, the wide slot width of SCAHSs was 1.2 m. Two batches of one-way concrete slabs were designed and their flexural performance was investigated. The first batch consisted of 12 concrete slabs (specimens of sets A1-A3) and the second batch consisted of 1 slab (specimen of sets A4). The load-bearing reinforcement of the slabs of set A1 was straight HRB400 steel bar. The load-bearing reinforcement of the concrete slab specimens of A2-A4 sets were SCAHSs, which was machined in the shape and size according to the ratio of the reinforcement bars of 1:2 as shown in Figure 2. According to the rise-span of the curved section of SCAHSs, the length of the concrete slabs was taken as 2,400 mm to ensure the confining effect



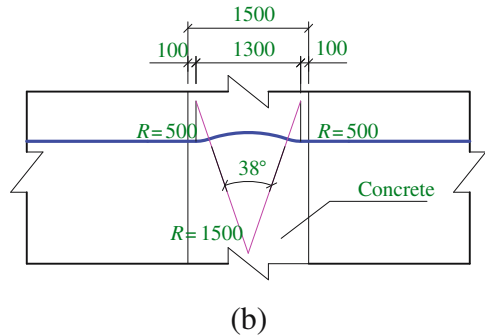


Figure 2: Shapes and dimensions of the SCAHSs in different sets of concrete slabs. (a) Type I for set A2 and (b) type II for sets A3 and A4.

**Table 1:** Design parameters for reinforcement in concrete slabs

t no.	no. Specimen no.	Reinforcement type	Load-bearing reinforcement	Number of reinforcements	Distribution of reinforcement	Number of slabs
	A1-a, A1-b, A1-c	Straight steel bars	C18@100	8	C12@100	3
	A2-a, A2-b, A2-c	Type I of SCAHSs	C18@100	8	C12@100	3
	A3-a, A3-b, A3-c	Type II of SCAHSs	C18@100	8	C12@100	3
	A4-a	Type II of SCAHSs	C10@120	9	C10@200	_

ote: C represents HRB400 steel bar

of the reinforcement on the concrete slab. The length-towidth ratio of a concrete slab ranged from 2 to 3. Considering the limitations of the test conditions, the width of the concrete slabs was taken as 900 mm for sets A1-A3 and 800 mm for set A4. The thickness of concrete slabs should be more than 80 mm, so the thickness of the slabs was designed as 200 mm for groups A1-A3 and 150 mm for set A4. The concrete slabs of sets A1-A3 was made of C25 and the concrete slab of set A4 was made of C30. The load-bearing reinforcement and distribution reinforcement were HRB400 steel bars with diameters of 18 and 12 mm, respectively. The design parameters of each one-way concrete slab are shown in Table 1, and the reinforcement diagram is shown in Figure 3. The whole process of fabricating the slabs was done in the component fabrication plant. Photographs of the reinforcement skeleton and formwork are shown in Figure 4. The actual dimensions of the slabs in groups A1-A3 after demolding are illustrated in Table 2. The actual dimensions of A4-a slab were 152 mm ×  $802 \text{ mm} \times 2,400 \text{ mm}.$ 

### 2.2 Material properties

Nine concrete cube specimens with a volume of 150 mm × 150 mm × 150 mm were poured simultaneously with the slab concrete to determine the actual strength of the concrete at the time of testing. The specimens were cured for more than 28 days. The measured compressive strength  $f_{cu}$  of C25 and C30 concrete cube specimens are listed in Tables 3 and 4, respectively. The axial compressive strength  $f_c$ , axial tensile strength  $f_{\rm t}$ , and elastic modulus  $E_{\rm c}$  of the concrete were calculated according to Eqs (1)-(3). Three HTRB400 steel bar specimens were taken and tested according to the material test standard [13]. The yield strength  $f_v$  and ultimate strength  $f_{\rm u}$  were 497.8 MPa and 594.5 MPa, respectively. The elastic modulus  $E_t$  of HTRB400 steel bar specimens was  $2.0 \times 10^5$  MPa.

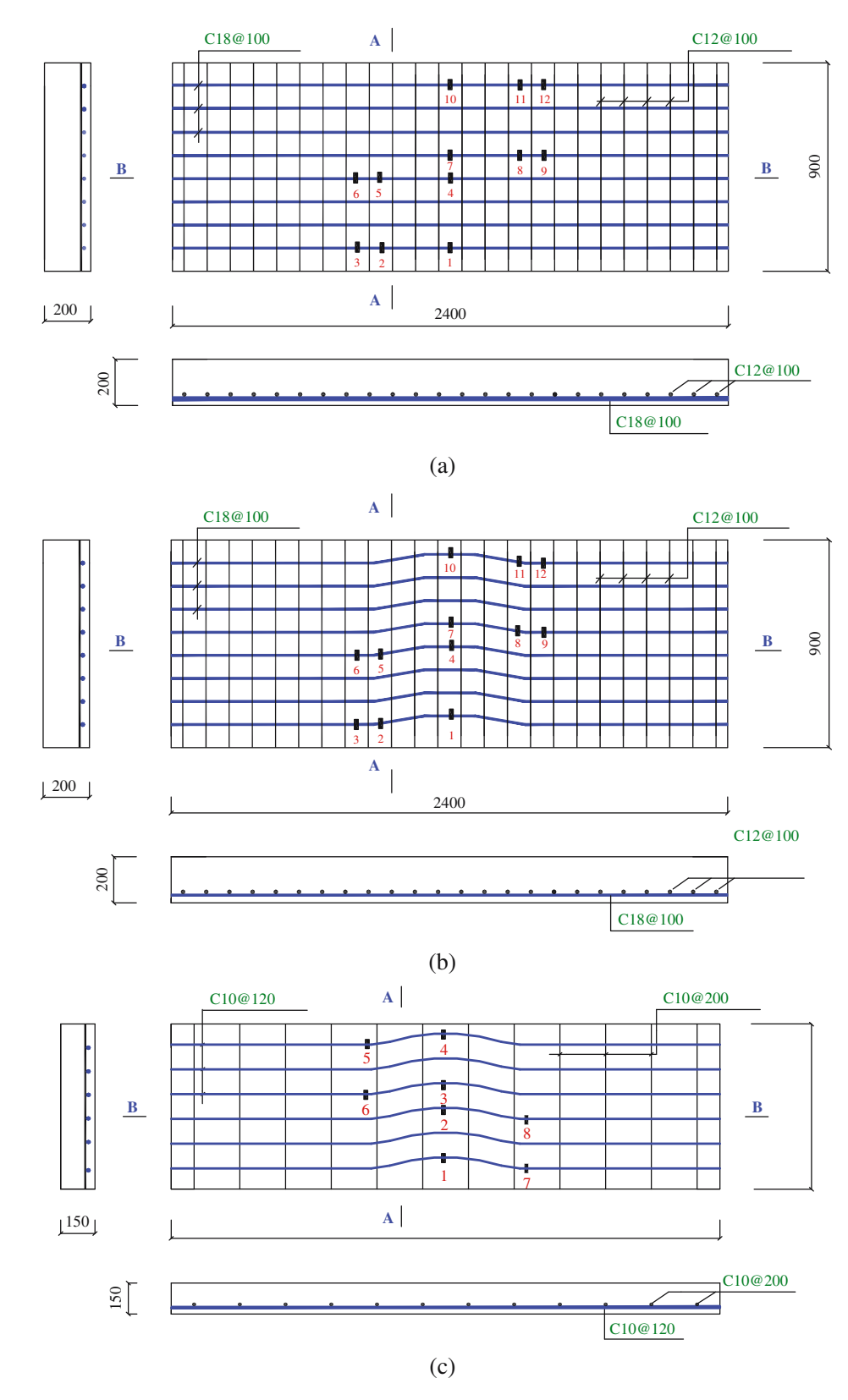
$$f_{\rm c} = 0.76 f_{\rm cu},$$
 (1)

$$f_{\rm t} = 0.26 f_{\rm cu}^{2/3},$$
 (2)

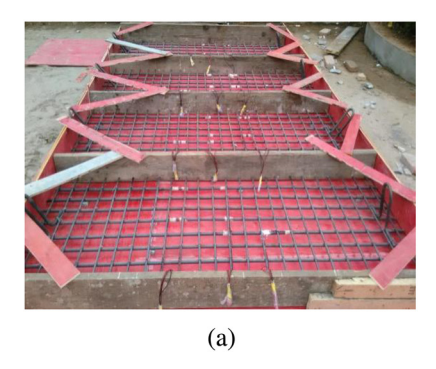
$$E_{\rm c} = \frac{10^5}{2.2 + \frac{34.7}{f_{\rm co}}}.$$
 (3)

### 2.3 Loading and measurement program

The loading method uses two points of symmetric loading. The arc section of SCAHSs was located between the two load points in a pure bending moment state, which ensures



**Figure 3:** Reinforcement diagram with strain gauge arrangement ("**—**" is the position of strain gauges). (a) Slabs of A1, (b) slabs of sets A2 and A3, and (c) slab of set A4.



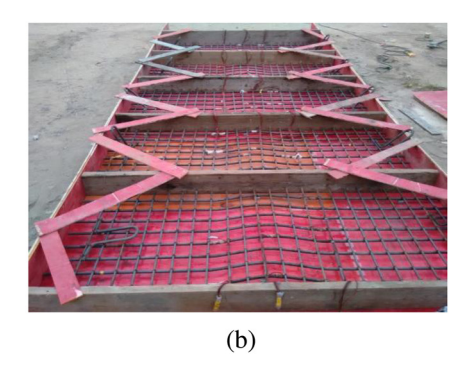


Figure 4: The formwork of one-way concrete slab specimens. (a) Distribution of straight steel bars and (b) distribution of SCAHSs.

Table 2: Actual dimensions of concrete slabs of sets A1-A3 (mm<sup>3</sup>)

**DE GRUYTER** 

Specimen no.	Actual size (mm³)	Specimen no.	Actual size (mm³)	Specimen no.	Actual size (mm³)
A1-a	220 × 910 × 2,403	A2-a	217 × 920 × 2,392	A3-a	210 × 920 × 2,415
A1-b	212 × 900 × 2,410	A2-b	201 × 910 × 2,402	A3-b	200 × 910 × 2,400
A1-c	205 × 910 × 2,400	A2-c	200 × 910 × 2,410	А3-с	200 × 905 × 2,415

that the maximum crack width appeared in the arc section of the reinforcement. The location of the supports and loading points are shown in Figure 5. The test setup is shown in Figure 6. The data collected for the tests were for reinforcement strain, concrete strain, mid-span deflection, and crack distribution and width. The exact locations of the concrete strain gauges are shown in Figure 7. In Figure 7(a), 5 points of concrete strain 1-5 were used to check the assumption of the plain section. In Figure 7(b), 20 points of concrete strain 1-20 were used to check the assumption of the plain section. Strain during the test was automatically collected every 5 s by a static strain gauge system. Deflection was measured by an electronic displacement meter, which was connected to the static strain gauge for loading along with the force transducer and was collected simultaneously with the strain.

### 3 Test results and discussion

### 3.1 Test phenomenon

#### 3.1.1 Damage processes and failure mode

Slab A1-b was taken as an example to illustrate the damage process of the concrete slab of set A1. When loaded to

Table 3: Strength and elastic modulus of C25 concrete (MPa)

	Measured compressive strength $f_{ m cu}$ of cube test blocks							$f_{\rm c}$ (MPa)	$f_{\mathrm{t}}$ (MPa)	E <sub>c</sub>
Test block No.	1	2	3	4	5	6	Average			
Strength values	23.7	25.2	24.0	25.7	25.3	26.0	25.0	19.00	2.22	2.79 × 104

Table 4: Strength and modulus of elasticity of C30 concrete (MPa)

1	Measured compressive strength of cube test blocks				f <sub>c</sub> (MPa)	f <sub>t</sub> (MPa)	E <sub>c</sub> (×10 <sup>4</sup> )
Test block no.	1	2	3	Average			
Strength values	37.09	37.95	38.06	37.70	28.65	2.92	3.13

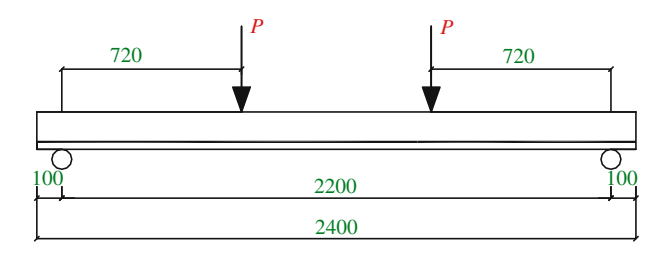


Figure 5: Supports and loading point locations.

 $53.5\,\mathrm{kN}$  (approx.  $0.127\,P_\mathrm{u}$ ,  $P_\mathrm{u}$  was the ultimate load,  $P_\mathrm{u}$  =  $420\,\mathrm{kN}$ ), a crack appeared on one side of the slab from the bottom of the span, and the mid-span deflection is very small, about 2 mm. Thereafter, the loading continued and the crack extended along the span in the transverse direction, while expanding vertically upwards and the mid-span deflection of the slab developed rapidly. When



Figure 6: Photograph of the actual loading.

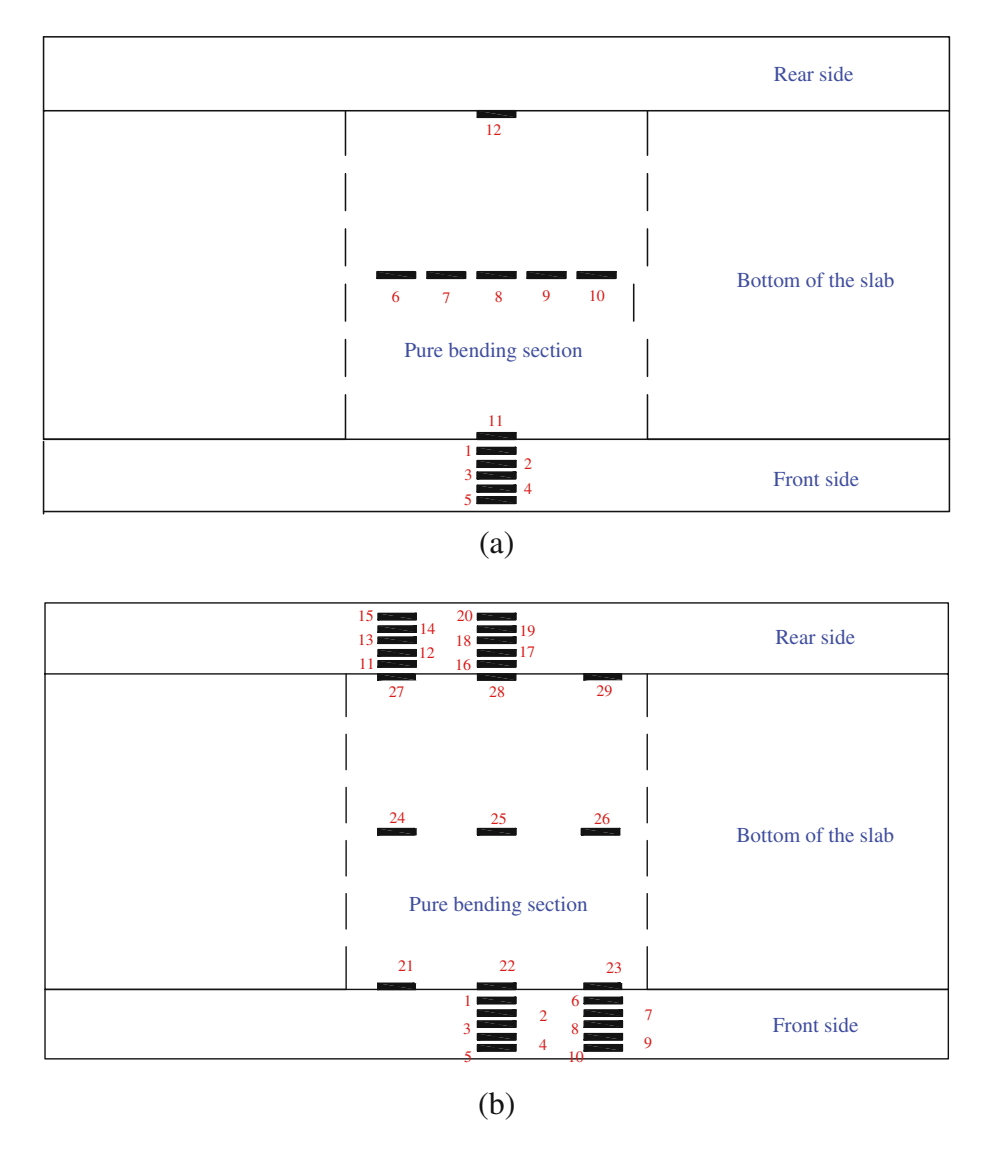


Figure 7: Concrete strain gauge locations ("=" is the concrete strain gauge locations). (a) Sets A1-A3 and (b) set A4.

loaded to 160 kN, the cracks at the bottom of the slab gradually increased. When loaded to 180 kN, the cracks at the bottom of the slab expanded along the transverse direction. When loaded to 330 kN, the mid-span deflection of the slab reached 12 mm and a diagonal crack appeared at the left end of the slab, and the longitudinal reinforcement was subjected to a tensile strain of 1,200; the load carrying capacity did not decrease significantly due to the influence of the longitudinal bar pinning force, but the slab deflection grew rapidly. When the mid-span deflection of the slab reached about 16 mm, the diagonal cracks developed rapidly toward concentration force point of action, the section cracks penetrated and diagonal tensile damage occurred. The longitudinal reinforcement did not reach yielding when the slab failed. The failure mode and crack morphology of slab A1-b are shown in Figure 8.

Slab A2-a was taken as an example to illustrate the damage process of the concrete slab of set A2. When loaded to 50.0 kN (0.128  $P_{\rm u}$ ,  $P_{\rm u}$  = 391 kN), a small crack appeared at the bottom of the slab near the loading point, and the midspan deflection of the slab was very small, about 1.7 mm. Thereafter, the loading continued, the mid-span deflection

of the slab developed rapidly, and the crack extended along the transverse direction of the bottom of the slab. When loaded to 120 kN, the cracks at the bottom of the slab gradually increased. When loaded to 140 kN, the cracks at the bottom of the slab expanded in the transverse direction. When loaded to 360 kN, the mid-span deflection of the slab reached 13 mm and a diagonal crack appeared at the right end of the slab, and the longitudinal reinforcement was subjected to a tensile strain of 1,400. The load carrying capacity did not decrease significantly due to the influence of the longitudinal bar pinning force, but the mid-span deflection of the slab grew rapidly. When the mid-span deflection of the slab reached about 16 mm, the diagonal cracks developed rapidly toward the concentrated force point of action, the section cracks penetrated and diagonal tensile damage occurred. The failure mode and crack development pattern of slab A2-a are shown in Figure 9.

Slab A3-a was taken as an example to illustrate the damage process of the concrete slab of set A3. When loaded to  $45.5 \, \mathrm{kN}$  (0.128  $P_\mathrm{u}$ ,  $P_\mathrm{u}$  = 355 kN), the bottom slab cracked at 1/3 of the purely bending part of the span, and the mid-span deflection of the slab was very small, about 1.4 mm.

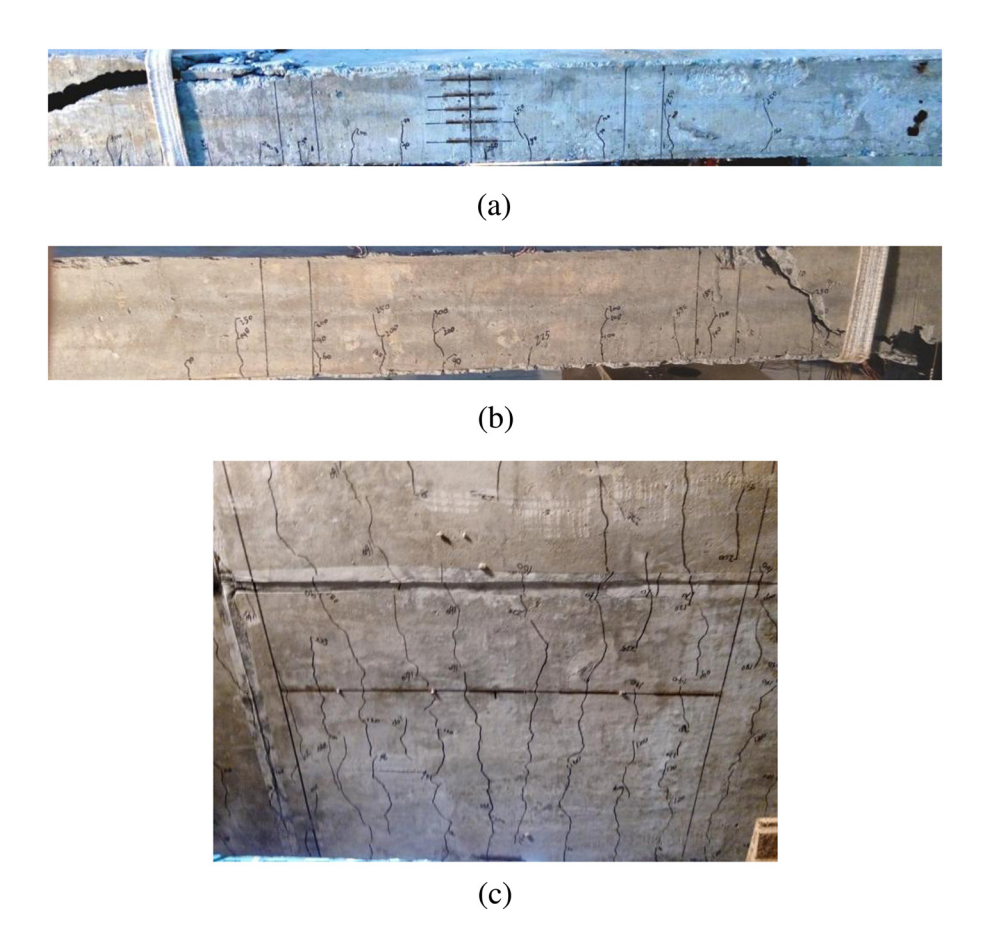


Figure 8: Damage and cracks in slab A1-b. (a) Front side, (b) rear side, and (c) bottom.

8 — Mei-Ling Zhuang et al. DE GRUYTER

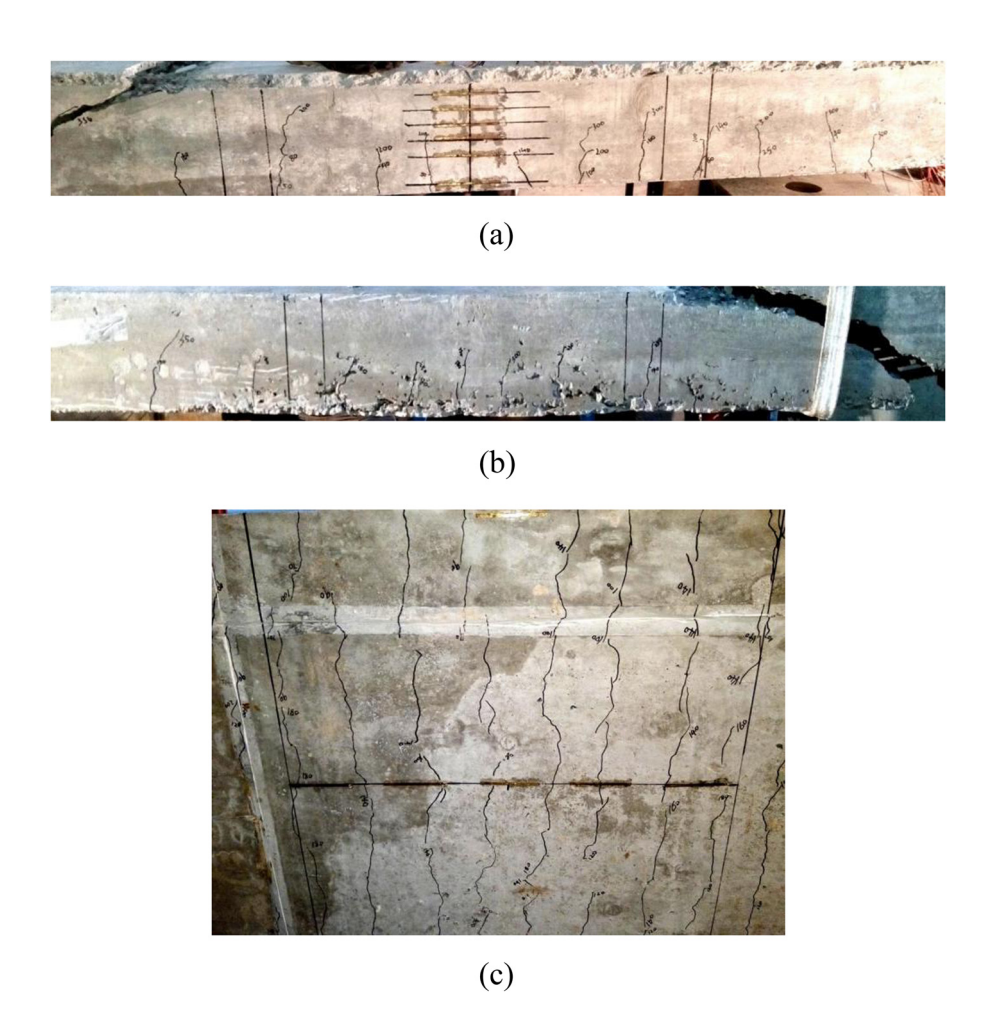


Figure 9: Damage and cracks in slab A2-a. (a) Front side, (b) rear side, and (c) bottom.

Thereafter, the loading continued and the mid-span deflection of the slab developed rapidly. When loaded to 80 kN, the cracks at the bottom of the slab extended along the transverse direction. When loaded to 100 kN, the cracks at the bottom of the slab increased and expanded rapidly. When loaded to 140 kN, the cracks at the bottom of the slab near the right loading point developed along the transverse direction. When loaded to 340 kN, the mid-span deflection of the slab reached 13 mm, a diagonal crack appeared at the right end of the slab, where the longitudinal reinforcement was subjected to a tensile strain of 1,200. The load carrying capacity did not decrease significantly due to the influence of the longitudinal bar pinning force, but the mid-span deflection of the slab grew rapidly. When the mid-span deflection of the slab reached about 16 mm, the diagonal crack developed rapidly toward the concentrated force point of action, the section cracks penetrated, and diagonal tensile damage occurred. The longitudinal reinforcement did not yield when the slab was damaged. The failure mode and crack morphology of slab A3-a are shown in Figure 10.

When loaded to 20 kN (0.235  $P_u$ ,  $P_u$  = 85 kN), cracks appeared at the bottom of the front edge of slab A4-a (inside concave side of the SCAHS), near the arc reinforcement anti-arc point area. While holding the load, cracks appeared at the bottom of the front edge of the slab (outside convex side of the SCAHS), near the arc reinforcement anti-arc point area, with a very small mid-span deformation of the slab, about 0.7 mm. Thereafter, the loading continued and the cracks developed rapidly. When loaded to 25 kN, the first transverse through crack appeared at the bottom of the slab. The same cracking loads were observed at the front and rear sides of the slab, indicating that the concave and convexity of the reinforcement had little effect on the cracking loads. When loaded to 35-40 kN, transverse bending cracks in the pure bending part basically appeared. After that, the cracks developed rapidly, and the development at the rear side of the slab (concave side of SCAHS) was slightly higher than that at the front side (convex side of SCAHS). It was also obvious that the deflection of the rear side of the slab (the concave side of

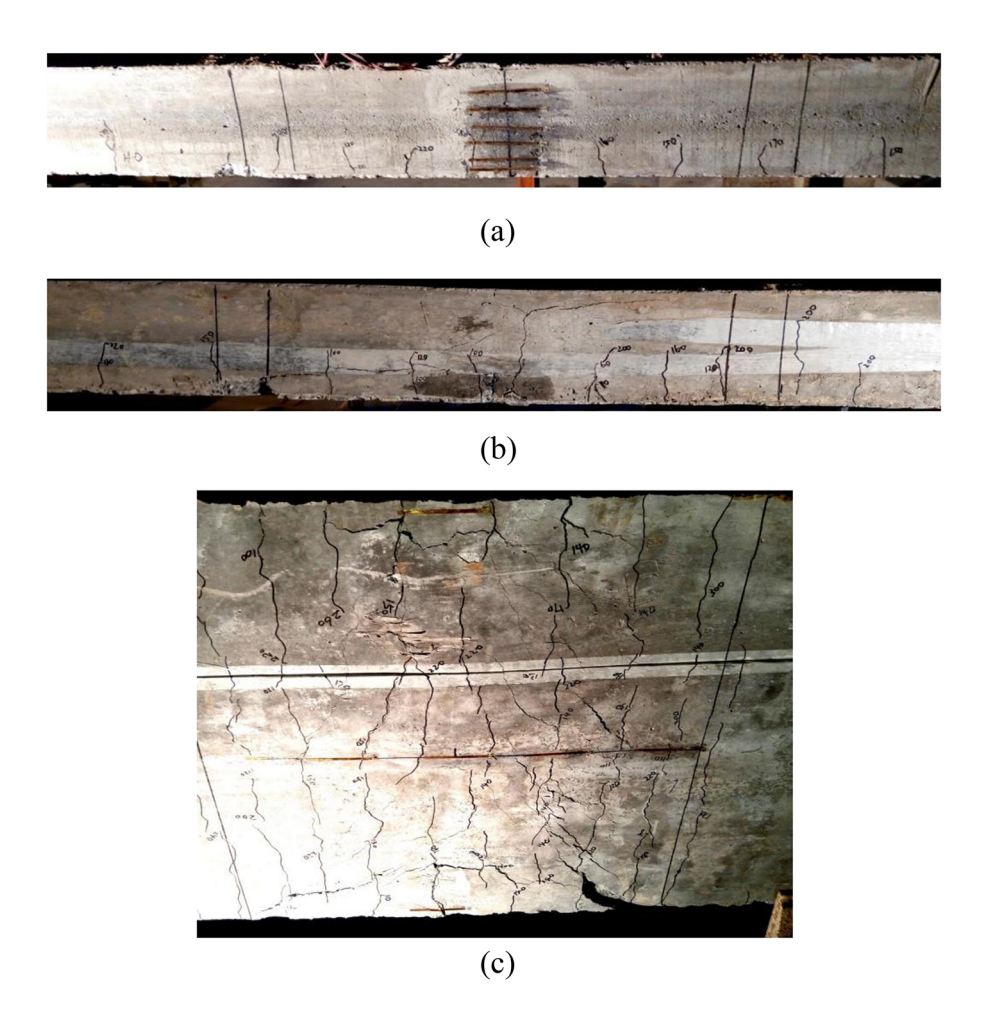


Figure 10: Damage and cracks in slab A3-a. (a) Front side, (b) rear side, and (c) bottom.

the SCAHS) was greater than that of the front side (the convex side of the SCAHS). This phenomenon indicated that the concave and convexity of the reinforcement had an effect on the crack orientation and the internal forces of the slab. When the reinforcement was stretched, it interacted with the concrete, resulting in an increase in the horizontal tensile stress of the concrete along the span direction on the concave side of the reinforcement, and a decrease in the tensile stress of the concrete on the convex side. When loaded to 65-70 kN, the mid-span deflection of the slab increased at a faster rate. When loaded to 80 kN, the mid-span deflection increased to 20 mm and the deflection increased at a slower rate. As the load increased, the crack width increased. When loaded to 85 kN without further loading and continuing to hold the load, the midspan deflection of the slab increased rapidly and eventually failed. When the slab was damaged, the critical crack in the front side of the slab (on the convex side of the SCAHS) was in the shape of an inverted eight, while the critical crack in the back side of the slab (on the concave side of the SCAHS) was in the shape of eight. The critical

cracks penetrated at the front and rear sides of the slab, forming two inclined concrete sections that led to the final damage of the slab. From the top of the slab, the cracks can be clearly seen running diagonally through the front and rear flanks. When the slab failed, the mid-span deflection of the slab exceeded 60 mm and the longitudinal reinforcement yielded. The failure mode and crack morphology of slab A4-a are shown in Figure 11.

### 3.1.2 Crack development pattern and damage mechanism

The cracks of the slabs of set A1 first appeared in the middle of the span, while the cracks of sets A2 and A3 (SCAHS reinforced concrete slabs) first appeared near the point of counter-arc of the curved reinforcement and the concentration force point of action. Cracks in the normal section of slab A1-b were mainly concentrated in the range of 1–2 times the slab thickness and extended outward from the two concentrated force points, *i.e.*, cracks in purely

10 — Mei-Ling Zhuang et al. DE GRUYTER

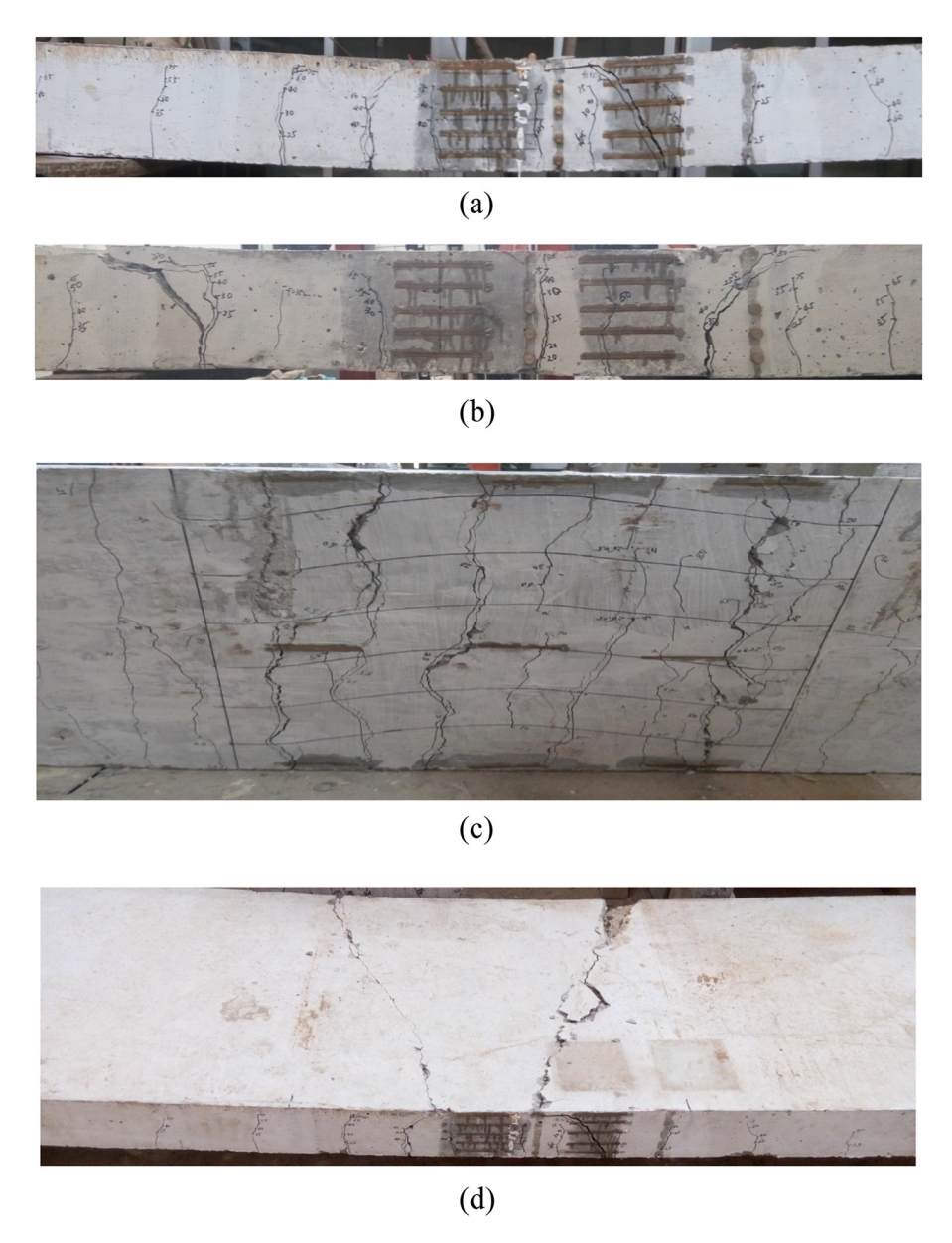


Figure 11: Damage and cracks in slab A4-a. (a) Front side (convex side of the SCAHS), (b) rear side, (c) bottom, and (d) top.

bending sections ranged in length from 2 to 4 times the slab thickness. All the cracks at the bottom of the slab extended more regularly along the direction perpendicular to the span of the slab. Slab A1-a had an asymmetrical force situation due to the uncompacted bar support at one end, so the cracks at the bottom of slab A1-a appeared to be inclined and the number of cracks on the front and rear sides differed greatly.

The number of cracks in the slabs of set A2 and set A1 was basically the same, but the crack distribution of the slabs of set A2 had two characteristics. One was that the correspondence between the cracks on the front and rear sides became worse, and the differences in sparsity and

density were more obvious, where the cracks on the concave side of the SCAHSs were sparser and the cracks on the convex side were denser. The second was that the splitting occurred during crack extension in the bottom of the slab, and the rocking decreased when crack expansion increased.

The cracks at the bottom of the slabs of sets A3 (650.0 mm vector span, 54.5 mm vector height) and A2 (500.0 mm vector span, 31.8 mm vector height) were developed significantly in terms of rocking amplitude and bifurcation, and the number of cracks increased. The difference in the number of cracks between the front and rear sides of the same slab increased. This was because the force direction of the SCAHS was at a certain angle to the longitudinal

direction of the slab, creating visible cracks in the SCAHS reinforced concrete slab within the curved reinforcement toward the concave and convex bends, and cracks along the SCAHS in the longitudinal direction at the bottom of the slab. The greater the vector height of the SCAHS, the more obvious this phenomenon was. In the case of straight steel bars reinforced concrete slabs, the cracks at the bottom of the slab basically developed along the transverse direction, with relatively straight distribution lines.

The cracking load of slab A4-a was 20 kN. The cracks of slab A4-a first appeared from the position of the anti-arc point of the curved arc reinforcement near the curved reinforcement on the side of the slab, and then gradually expanded to the middle of the slab along the transverse direction. Subsequently, the crack width then increased and the crack height on the front and rear sides increased, and the crack height on the rear side of the slab (the concave side of the SCAHS) was significantly higher than that on the front side (the convex outer side of the SCAHS), when the concrete area in the compression zone was smaller. When the load reached 80 kN holding load, a paracord crack appeared at the starting point in the middle of the curved arc segment of the longitudinal reinforcement. When the load reached the destructive load, two main cracks near the counter-arc point of the side arc reinforcement on the front of the slab gradually formed an inverted eight crack pattern, while the two main cracks near the anti-arc point of the curved arc reinforcement gradually formed a crack pattern of eight; holding the load, these four cracks formed a critical crack leading to damage. After unloading the loading equipment in the upper part of the slab, the critical cracks on the front and rear sides can be observed to penetrate in the upper part, indicating the formation of the damage surface (Figure 12).

The mechanism of damage surface formation was complex and was influenced by the following three effects.

- (1) Vertical bending effect. Vertical bending moment effect, the upper part of the slab was compressed and the lower part was pulled.
- (2) Horizontal additional bending effect. When the slab was loaded, the curved arc reinforcement at the bottom of the slab had a tendency to straighten, the rear side of the

- slab (the concave side of the SCAHS) was under tension and the front side of the slab was under pressure.
- (3) Torsion effect. In the mid-span reinforcement arc section of the slab, the bending of the reinforcement arc caused the reinforcement rate on the rear side of the slab (the concave side of the reinforcement) to be smaller than that on the front side, and the transverse deflection of the rear side of the slab under the load was much larger than that of the front side of the slab, resulting in the tendency of the slab to turn backward. The vertical load applied on the inclined slab surface further increased this inclination, resulting in the torsional effect of backward turning of the slab at the loading point (Figure 12). In the mid-span section, the SCAHS was stretched, causing the concrete at the bottom of the slab to be subjected to horizontal extrusion force in the backward direction, and this horizontal force caused a reverse torsional effect in the middle of the slab.

At the early stage of loading, under the influence of vertical bending effect and horizontal additional bending effect, transverse cracks appeared first at the rear side of the bottom of the slab, and extended upward and forward with the increase in load. The crack direction appears to be more wavering due to the interaction between SCAHS and concrete. The torsion effect had little effect in the early and middle stages of loading. Under the effect of vertical bending, the cracks at the bottom of the slab were through. Under the effect of additional horizontal bending, the cracks on the front side of the slab developed at a height slightly behind the rear side of the slab (Figure 11(a) and (b)). In the later stage of loading, the torsional effect gradually increased and the slab was in tension on the front, rear, and bottom sides and in compression on the top side, with torsional diagonal cracks appearing on the front and rear sides, which were positioned between the mid-span and the loading point. At the bottom, on the other hand, no diagonal cracking occurred due to the bending and pulling transverse cracks that already existed in the crack-through. Under the failure load, the concrete in the top compressed zone reached the ultimate compressive strain and failed (Figure 11d).

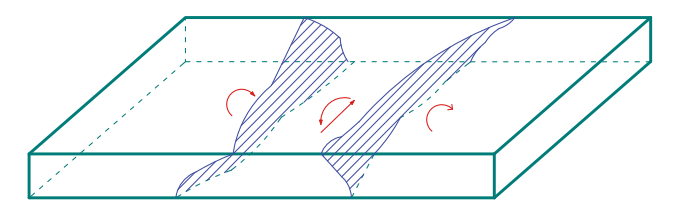


Figure 12: Schematic diagram of damage surface of slab.

### 3.2 Characteristic loads and load-mid-span deflection curves

#### 3.2.1 Characteristic loads

The cracking load and ultimate load of each slab are listed in Table 5. Comparison of the observed cracking loads

Table 5: Cracking and ultimate loads of each slab (kN)

Specimen no.	Specimen no.		A1				A2				А3		A4
	A1-a	A1-b	А1-с	Average	A2-a	A2-b	A2-c	Average	А3-а	A3-b	А3-с	Average	A4-a
Cracking load Ultimate load	(60.0) (335)	53.5 420.0	50.5 376.0	52.0 398.0	50.0 391.0	43.3 367.0	47.5 396.0	46.9 385.0	45.5 355.0	42.4 365.0	48.5 375.0	45.5 365.0	20.0 85.0

Note: The average load of the slabs of set A1 is the average load of slabs A1-b and A1-c.

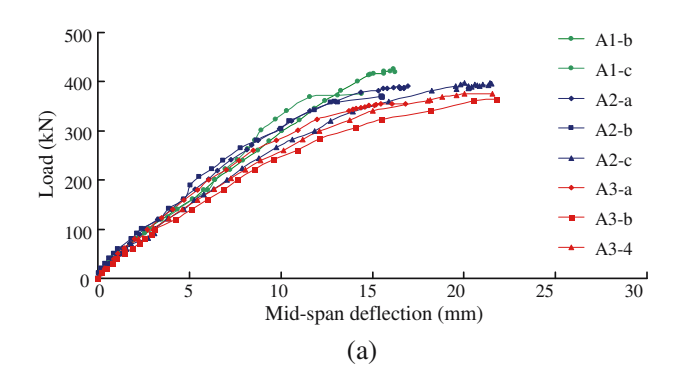
indicated that the starting cracking loads of the slabs with SCAHSs of sets A2 and A3 were lower than those of set A1, and the cracking loads of the SCAHS with higher vector heights were also lower. The reason for this was that when SCAHS were placed horizontally, the local reinforcement ratio at the edges of the convex SCAHS slabs was higher, while the local reinforcement ratio at the edges of the concave SCAHS slabs was lower, and the tensile capacity of the SCAHS reinforced slabs was lower than that of the straight reinforcement-reinforced slabs, which led to lower cracking loads in the SCAHS reinforced slabs. The longitudinal reinforcement ratio of the slabs was 1.27% and the effect of reinforcement on the cracking load was about 9%. Therefore, the decrease in cracking load was smaller for slabs reinforced with SCAHSs compared to slabs reinforced with straight reinforcement. Since all the slabs of sets A1-A3 undergo diagonal tensile damage, the ultimate loads of all the slabs were close to each other, except for slab A1-a, which was slightly higher due to the loosening of the support at one end.

#### 3.2.2 Load-mid-span deflection curves

The load—mid-span deflection curves of the slabs are shown in Figure 13. The load—mid-span deflection curves of the three slabs of set A1 were very close to each other in the early stage of loading, and the differences were larger near the time of damage, but they were still within the normal range of material dispersion effect and test error. Slab A1-a had a lower cracking load and lower ultimate load due to the un-compacted support at one end. The patterns of slabs A1-b and A1-c were essentially similar. The load—mid-span deflection curves of the three slabs of sets A2 and A3 had similar shape and ultimate load, but there were some differences in the mid-span deflections for the same load.

At the beginning of loading, the load–mid-span deflection curve of the A4-a plate increases linearly, with an inflection point at 20 kN, where the curve converges to the deflection axis. When the load reached between 70 kN and 85 kN, the curve fluctuated up and down, and the deflection continued to increase, but the load bearing capacity of slab A4-a

stopped increasing. The cracking load, yield load, and ultimate load of the slab A4-a were 20, 65, and 85 kN, respectively. After yielding of the reinforcement, the stiffness of slab A4-a degraded less compared to the slab with straight steel bars for the same strain increment because the reinforcement was stretched obliquely. When loaded to 75 kN with a mid-span deflection of about 18.5 mm, the reinforcement entered the strengthening phase and thus the load carrying capacity increased. When loaded to 85 kN, the crack with the largest width and the longest extension developed rapidly into a critical crack under the combined effect of the positive stress caused by the bending moment and the local pressure caused by the straightening of the SCAHSs, and the reinforcement through this crack entered the strengthening phase. When the stress of the first SCAHS at the rear side reached the ultimate strength into the descending section, the load carrying capacity decreased leading to damage.



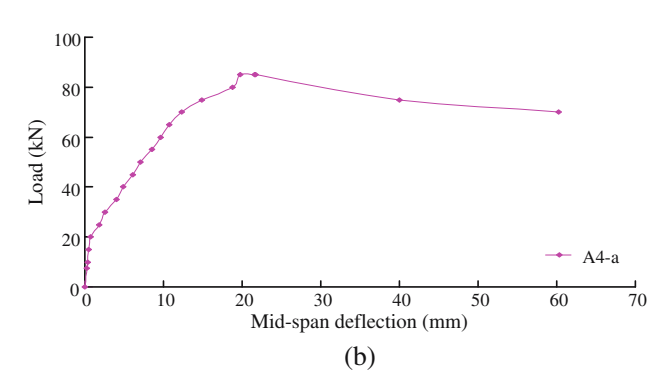


Figure 13: Load-mid-span deflection curves. (a) A1-A3, (b) A4.

For the same load, the flexural stiffness of the slab reinforced with SCAHSs was smaller and the mid-span deflection was larger compared to the slab reinforced with straight reinforcement. The flexural stiffness of the slab reinforced with SCAHSs decreased as the vector height of the SCAHSs increased. The average mid-span deflection of the slabs of set A3 (650.0 mm vector span and 54.5 mm vector height) was about 23 mm at ultimate load, which was 53% greater than that of the slabs of set A1. This indicated that the slab reinforced with SCAHSs had a better deformation capacity than those reinforced with straight reinforcement when damage occurred in the diagonal section.

### 3.3 Crack spacing and width

#### 3.3.1 Measured crack spacing

Table 6 presents the measured values of crack spacing for the purely curved section of each slab. As the vector height of the SCAHSs increased, the number of cracks increased and the average crack spacing decreased. Except for slab A1-c, the maximum crack spacing ranged from 162 to 195 mm. The minimum crack spacing for most of the slabs ranged from 50 to 60 mm. Slab A3-b showed a crack spacing of only 25 mm. This was due to an intersection angle between the tangential direction of the SCAHSs and the span direction of the slab, which reinforced the anchorage of the reinforcement along the longitudinal direction. If the vector height of the SCAHSs was greater, the tangential angle of intersection with the longitudinal span of the slab would be greater, the anchoring effect of the reinforcement along the longitudinal direction would be stronger, and the crack spacing would be smaller.

### 3.3.2 Comparison of measured crack spacing and calculated crack spacing

In the design specification for hydraulic concrete structures (DL/T5057-2009) [14], the maximum crack width is calculated according to the following equations:

$$w_{\text{max}} = \alpha_{\text{cr}} \psi \frac{\sigma_{\text{sk}} - \sigma_0}{E_{\text{s}}} l_{\text{cr}}, \tag{4}$$

$$\psi = 1 - 1.1 \frac{f_{\text{tk}}}{\rho_{\text{te}} \sigma_{\text{sk}}},$$
 (5)

$$l_{\rm cr} = \left(2.2c + 0.09 \frac{d}{\rho_{\rm te}}\right) v$$
 (20 mm \le c \le 65 mm), (6a)

$$l_{\rm cr} = \left[65 + 1.2c + 0.09 \frac{d}{\rho_{\rm te}}\right] v \quad (65 \text{ mm} \le c \le 150 \text{ mm}), \quad (6b)$$

Table 6: Measured crack spacing in purely curved section of each slab (mm)

No.	Part	Measured crack spacing S	Average c	rack spacing S <sub>a</sub>	
A1-a	Front side	195, 172, 80	149	132	_
	Rear side	155, 80, 120, 106	115		
A1-b	Front side	103, 100, 100, 89, 105, 110, 176, 100, 156, 146, 186	125	124	132
	Rear side	84, 125, 100, 110, 150, 136, 144, 55, 190	122		
А1-с	Front side	180, 212, 110, 262, 90, 232, 100, 110	161	139	
	Rear side	145, 130, 46, 210, 100, 130, 100, 102, 67, 150, 90	116		
A2-a	Front side	141, 165, 85, 172, 82, 105, 100, 106, 135, 66	116	128	119
	Rear side	190, 140, 111, 90, 133, 175	140		
A2-b	Front side	90, 115, 125, 150, 120	120	122	
	Rear side	170, 132, 102, 95, 103, 145	124		
A2-c	Front side	97, 88, 135, 162, 131, 65, 60, 160, 147, 66, 75, 100	107	108	
	Rear side	125, 155, 46, 70, 165, 90, 108, 111, 130, 90, 105	109		
A3-a	Front side	175, 170, 130, 95, 50, 110, 115, 85, 100, 85	112	114	111
	Rear side	190, 80, 130, 84, 100, 70, 45, 100, 105, 125, 160, 200	116		
A3-b	Front side	100, 110, 145, 148, 75, 130, 25, 67, 31, 142, 167, 172	109	103	
	Rear side	95, 110, 128, 115, 120, 87, 55, 103, 60, 77, 95, 95, 115	97		
А3-с	Front side	133, 165, 25, 185, 106, 180, 58, 98, 155, 167, 97, 152	117	115	
	Rear side	140, 109, 100, 97, 135, 170, 85, 115, 120, 70, 120, 80	112		
A4-a	Front side	180, 125, 104, 140, 68, 98, 110, 183	109	117	117
	Rear side	185, 85, 142, 185, 80, 115, 100, 105	125		

where  $\alpha_{cr}$  is the coefficient considering the force characteristics of the member and  $\alpha_{\rm cr}$  is 1.90 for bending members;  $\psi$ is the strain unevenness factor for longitudinal tensile reinforcement between cracks;  $\sigma_{sk}$  is the stress in longitudinal tensile reinforcement of the member calculated according to the standard combination of loads;  $\sigma_0$  is the initial stress in the reinforcement;  $l_{cr}$  is the average crack spacing;  $E_{s}$  is the modulus of elasticity of the reinforcement;  $f_{tk}$  is the standard value of the axial tensile strength of concrete; c is the distance from the outer edge of the outermost longitudinal tensile reinforcement to the bottom edge of the tensile zone; d is the diameter of the reinforcement;  $\rho_{\rm te}$  is the effective reinforcement ratio of the longitudinal tensile reinforcement,  $\rho_{te} = A_s/A_{te}$ ;  $A_{te}$  is the area of the effective concrete section in tension;  $A_s$  is the cross-sectional area of the longitudinal reinforcement in the tension zone; and  $\nu$  is a coefficient that takes into account the surface shape of the reinforcement.

For bending members, the reinforcement stress  $\sigma_{sk}$  is calculated using Eq. (7).

$$\sigma_{\rm sk} = \frac{M_{\rm k}}{0.87 A_{\rm s} h_0},\tag{7}$$

where  $M_k$  is the value of the bending moment calculated according to the standard combination of load effects; and  $h_0$  is the effective height of the cross-section.

In the Design Code for Hydraulic Concrete Structures (SL191-2008) [15], the maximum crack width is calculated according to the following equation:

$$l_{\rm cr} = \alpha_0 \frac{\sigma_{\rm sk}}{E_{\rm s}} \left[ 30 + c + \frac{0.07d}{\rho_{\rm te}} \right],$$
 (8)

where  $a_0$  is the comprehensive influence coefficient considering the force characteristics of the member and the long-term effect of the load,  $a_0$  = 2.1 for bending members; and c is the distance from the outermost longitudinal tensile reinforcement outer edge to the edge of the tensile zone, c is taken as 65 mm if c > 65 mm.

The average crack spacing of the slab reinforced with straight steel bars calculated using Eq. 6(a) in the specification DL/T5057-2009 was 120 mm. Compared with the measured crack spacing in Table 6, the calculated crack spacing was slightly less than the measured spacing of the slabs of sets A1 and A4, greater than that of the slabs of set A3, which was almost the same as the measured spacing of the slabs of set A2.

#### 3.3.3 Variation in crack width with load

As the test was a short-term loading test, the calculated crack widths were net of the effects of long-term loading,

i.e., the values calculated by the current code equation divided by an expansion factor of 1.5 for the effects of long-term loading. Comparison of the measured and calculated maximum crack widths of the slabs of sets A1-A3 are listed in Table 7. For the same load, the crack widths of the slabs reinforced with SCAHSs were larger than those of the slabs reinforced with straight reinforcement. The measured maximum crack width of the slab reinforced with SCAHSs increased as the vector height of SCAHSs increased. The measured average maximum crack widths increased to about 1.0-1.3 times for the slabs of set A2 and to about 1.0-1.5 times for the slabs of set A3 compared to the slabs of set A1. For slabs reinforced with straight reinforcement, the maximum crack width calculated using the equations from the code SL191-2008 was slightly larger than the measured average maximum crack width, indicating that the test results were credible. The maximum crack width calculated using the equations in the specification DL/T5057-2009 was smaller than the measured average maximum crack width. The maximum crack width calculated using the equations in the code SL191-2008 was close to the measured maximum crack width of the slabs of set A2 and differed greatly from those of set A3, indicating that the equations for the maximum crack width in code SL191-2008 cannot be directly applied to SCAHSs reinforced concrete slabs.

Comparison of the measured and calculated maximum crack widths for the slabs of set A4 are listed in Table 8. If it was assumed that the maximum crack width calculated using the code equations was a true reflection of the test results for the slabs reinforced with straight reinforcement,

**Table 7:** Comparison of the measured and calculated maximum crack widths of the slabs of sets A1–A3

Load	Rebar			W (mm	1)		W <sub>SL</sub>	W <sub>DL</sub>
(kN)	stress (MPa)	A1	A2	A2/A1	А3	A3/A1	(mm)	(mm)
120	152	0.10	0.10	1.00	0.10	1.00	0.11	0.05
140	177	0.10	0.13	1.30	0.15	1.50	0.13	0.07
160	202	0.13	0.15	1.15	0.15	1.15	0.14	0.09
180	227	0.13	0.15	1.15	0.18	1.38	0.16	0.11
200	253	0.15	0.18	1.22	0.22	1.44	0.18	0.13
220	278	0.18	0.18	1.00	0.25	1.39	0.20	0.15
225	284	0.20	0.22	1.10	0.25	1.25	0.21	0.16
240	303	0.20	0.23	1.10	0.30	1.50	0.22	0.17

Note: The average crack width for the slabs of set A1is the average crack widths of slabs A1-b and A1-c; A2/A1 and A3/A1 are the measured average maximum crack width ratios for the slabs of sets A2 and A1 and sets A3 and A1 respectively; W is the average of the measured maximum crack width;  $W_{\rm DL}$  is the maximum crack width calculated using the equations in the specification DL/T5057-2009;  $W_{\rm SL}$  is the maximum crack width calculated using the equations in the code SL191-2008.

**Table 8:** Comparison of the measured and calculated maximum crack widths of slab A4-a

Load (kN)	W (mm)	W <sub>DL</sub> (mm)	W/W <sub>DL</sub>	W <sub>SL</sub> (mm)	W/W <sub>SL</sub>
30	0.15	0.07	2.02	0.13	1.12
40	0.18	0.12	1.50	0.18	1.00
50	0.20	0.17	1.20	0.22	0.91
60	0.35	0.21	1.64	0.27	1.30

it can be seen that the maximum crack widths for the slab reinforced with SCAHSs was greater than those for the slab reinforced with straight reinforcement. The ratios of the measured crack width to the crack width calculated using the code SL191-2008 ranged from 0.9 to 1.3.

### 3.4 Strain distribution along the height of the cross-section

The assumption of the plain section was checked by testing the lateral concrete strains with strain gauges and handheld strain gauges, respectively. The reason was that when cracks passed through the strain gauge they can cause damage to the gauge resulting in inaccurate test results. Strain gauge measurements were taken before the crack passed through the strain gauge and thereafter by hand held strain gauge. The strain distribution along the height of the cross section at the front side of slabs of sets A1–A3 is described in Figure 14(a)–(c). The strain distribution along the height of the cross section at the rear side of slabs of set A4 is described in Figure 14(d). When the load was small, the strain was linearly distributed along the height of the cross-section; as the load increased and the concrete in the tension zone continued to crack, the strain was not perfectly linearly distributed along the height of the cross section, but can basically be considered to satisfy the assumption of the plain section.

### 4 Analysis of the synergistic tensile work of the SCAHS and concrete

When working in conjunction with concrete, the force state and damage characteristics of the SCAHSs were significantly different from those of straight reinforcement. In order to further understand the force performance of the SCAHSs reinforced concrete slabs, a mechanical sketch of the SCAHSs and concrete in synergistic tension was established to analyze their working characteristics.

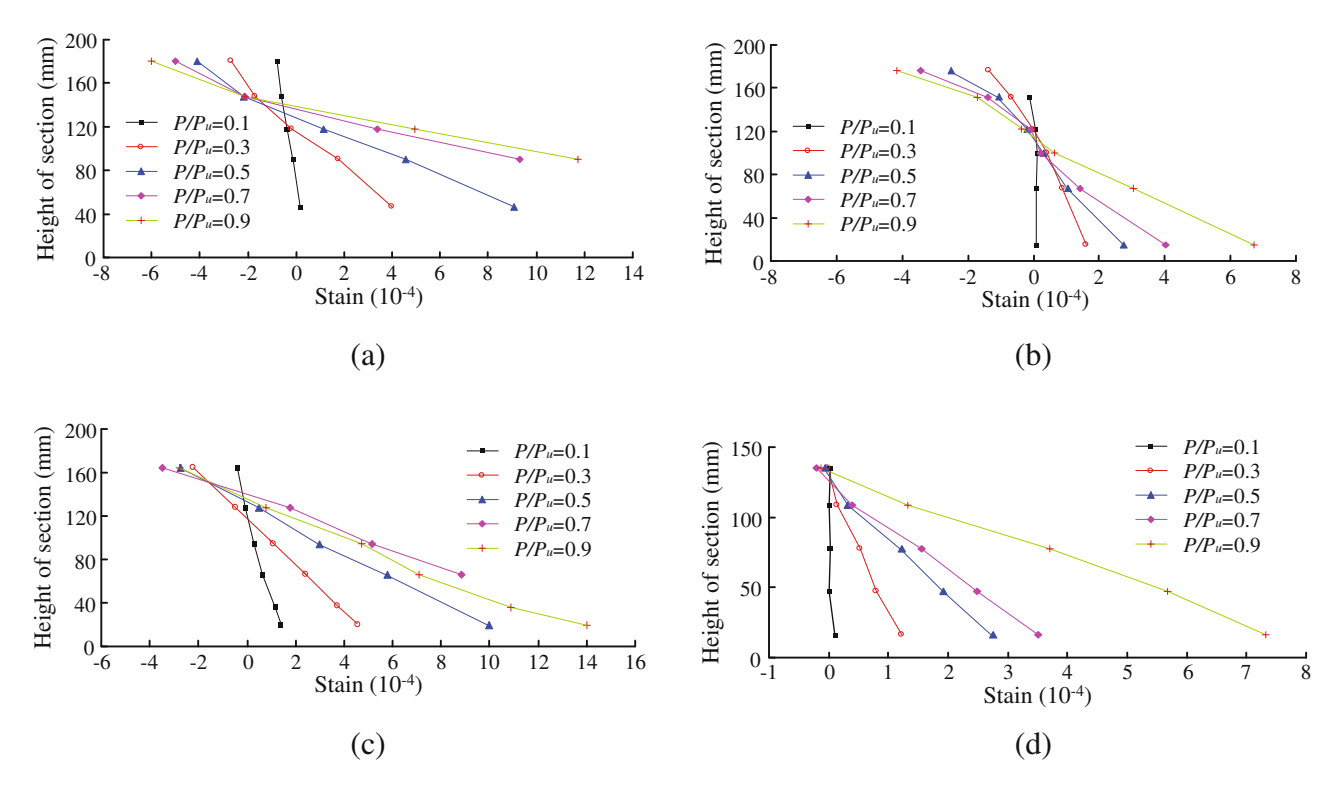


Figure 14: Strain distribution along the height of the cross section. (a) Slab A1-b, (b) slab A2-a, (c) slab A3-a, and (d) slab A4-a.

### 4.1 Tensile analysis of concrete members with a single SCAHS

The action of a SCAHS in the concrete is described in Figure 15. Let the member be l in length, b and h in section width and height, respectively, and be reinforced with a SCAHS of sagittal height  $h_a$  and cross-sectional area  $A_{\rm SC}$ . The ends were subject to axial tension P. The SCAHS had two distinctly different characteristics compared to the straight steel bar. When the SCAHS was in tension, it had a tendency to be straightened, producing an extrusion force on the concrete down the middle and up the sides, forming the additional bending moment  $M_{\rm T}$ . Each section of the SCAHS was at an angle to the axial tension and it was not fully functional.

### 4.1.1 Additional bending moment

In axially stressed members, assuming equal strains in the section before cracking, the stress distribution in section II—I and any flat straight section II—II where the apex of the arc-shaped section of the reinforcement was located is shown in Figure 16(a). The reinforcement stress  $\sigma_s$  and concrete stress  $\sigma_c$  satisfied Eq. (9).

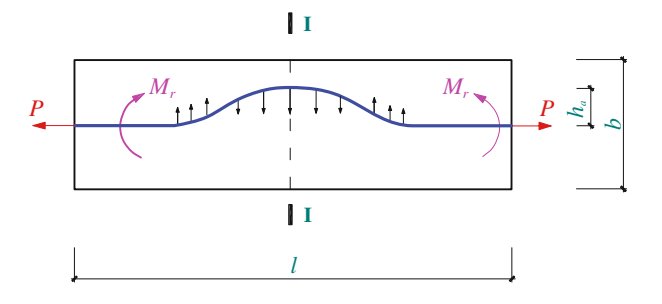


**Figure 15:** Schematic diagram of the action of a SCAHS in the concrete.

$$\sigma_{\rm s} = \frac{E_{\rm s}}{E_{\rm c}} \sigma_{\rm c}. \tag{9}$$

Let  $\alpha = E_s/E_t$ , and then Eq. (9) can be rewritten as follows:

$$\sigma_{\rm s} = \alpha \sigma_{\rm c}$$
. (10)

The part between sections I–I and II–II was analyzed as an isolated body (Figure 16(a)). The concrete stresses at both ends canceled each other out. The two non-coincident reinforcement tensions formed a pair of force couples, generating a bending moment  $M_{\rm r}$  in the section, as shown in Figure 16(b). The average stress in the member, the stress in the reinforcement, and the additional bending moment in the member satisfied the following equations:

$$\sigma_{\rm c} = \frac{P}{bh + (\alpha - 1)A_{\rm SC}} = \frac{P}{A_{\rm o}},$$
 (11)

$$P_{\rm S} = \sigma_{\rm S} A_{\rm SC} = \frac{\alpha A_{\rm SC} P}{A_0}, \tag{12}$$

$$M_{\rm r} = P_{\rm s} h_{\rm a} = \frac{\alpha A_{\rm sc} P}{A_{\rm o}} h_{\rm a}.$$
 (13)

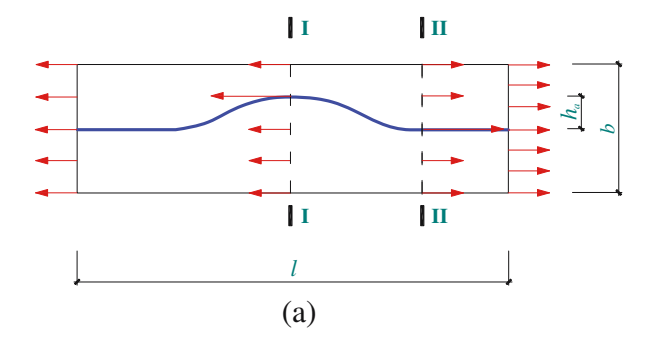
### 4.1.2 Cracking loads

### 4.1.2.1 Cracking load on the section where the arc top of the reinforcement is located

On the lower side of the member, the tensile stress from the axial tension and the tensile stress from the additional bending moment  $M_{\rm r}$  were superimposed to produce a maximum tensile stress  $\sigma_{\rm t, max}$ , which can be calculated using Eq. (14).

$$\sigma_{t,\text{max}} = \frac{P\alpha A_{\text{sc}} h_a}{A_0} / \left(\frac{b^2 h}{6}\right) + \frac{P}{A_0} = \frac{P}{A_0} \left(1 + \frac{6\alpha A_{\text{sc}} h_a}{b^2 h}\right).$$
 (14)

Let the maximum tensile stress be equal to the standard value of the concrete tensile strength. Then, the



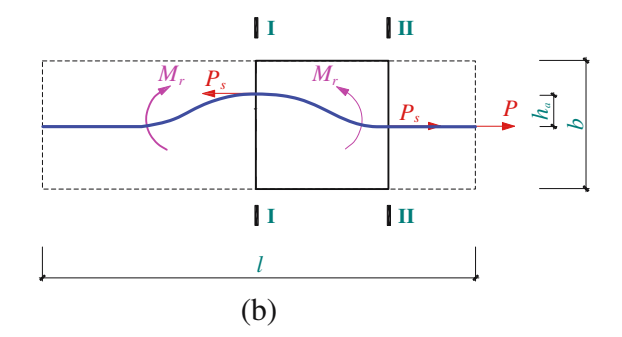


Figure 16: Force state of axially tensioned members with a SCAHS. (a) Axially tensioned members and (b) the curved section of the reinforcing bar.

cracking load  $P_{cr}$  at the top of the SCAHS arc can be obtained as follows:

$$P_{\rm cr} = \frac{f_{\rm tk}}{\gamma_{\rm a}} A_{\rm o}, \tag{15}$$

$$\gamma_{\rm a} = 1 + \frac{6\alpha A_{\rm sc} h_{\rm a}}{h^2 h},\tag{16}$$

where  $y_a$  was defined as the influence factor of the SCAHS.

In the derivation of Eq. (14), the effect of the SCAHS was ignored in the calculation of the modulus of the flexural section within the direction of the additional bending moment due to the reinforcement being in the center of the section form and the small reinforcement ratio.

### 4.1.2.2 Cracking load on an arbitrary section of the SCAHS

As shown in Figure 17, the SCAHS was at an angle to the axial tension between the top of the SCAHS arc and the flat straight section of the SCAHS. The angle of any taken section was  $\theta$ , and the vertical distance between this section and the flat straight section of the SCAHS was  $h_y$ . Let the tensile stress in the reinforcement of the section be  $\sigma_s$ . The component in the direction of tension was  $\sigma_s \cos \theta$ . The axial stiffness provided by the reinforcement was discounted accordingly, *i.e.*, the average stress in the concrete of the section when no additional bending action was considered is as follows:

$$\sigma_{\rm c} = \frac{F}{A_{\rm o}'} = \frac{P}{bh + A_{\rm sc}(\alpha\cos\theta - 1)}.$$
 (17)

The maximum tensile stress after considering the superposition of the additional bending moment effect was

$$\sigma_{\rm t, max} = \frac{P}{bh + A_{\rm sc}(\alpha \cos \theta - 1)} \left[ 1 + \frac{6\alpha A_{\rm sc} h_{\rm y}}{b^2 h} \right]. \quad (18)$$

The cracking load equation was modified as follows:

$$P_{\rm cr} = \frac{f_{\rm tk}}{V_{\rm v}} A_{\rm o}'. \tag{19}$$

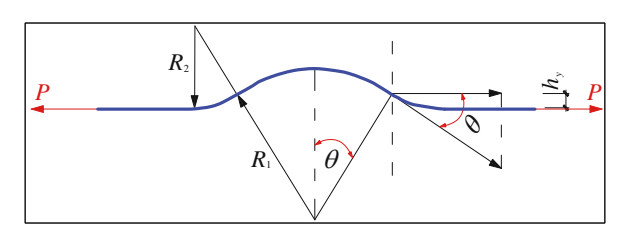


Figure 17: Force analysis of the arc section of the SCAHS.

As the section was chosen arbitrarily, the same was applied to a straight section of the SCAHS, when  $\theta = 0$ ,  $\gamma_v = \gamma_a$ .

#### 4.1.3 Location of the first crack

Assume that the tensile strength of concrete in each section was the same and the first crack appeared in the section with the lowest cracking load  $P_{\rm cr}$ . Let the radius of curvature of the middle-curved section of the SCAHS be  $R_1$ , corresponding to a maximum fillet angle of  $2\theta_0$ , and the radius of the curved section at both ends be  $R_2$ , corresponding to a fillet angle of  $\gamma_0$ . An arbitrary section was chosen in the slightly curved arc section. The intersection of the section with the reinforcement was point A. The angle of the arc segment between point A and the top of the arc was  $\theta$ . The angle of the flat segment between point A and the beginning of the flat segment was  $\gamma$  (Figure 18). The height from point A to the flat segment of the reinforcement can be calculated as follows:

$$\begin{cases} h_{y} = R_{1}(\cos \theta - \cos \theta_{0}) + R_{2}(1 - \cos \gamma_{0}) & (\theta \leq \theta_{0}) \\ h_{y} = R_{2}[1 - \cos(\gamma_{0} - \gamma)] & (\gamma \leq \gamma_{0}). \end{cases}$$
 (20)

Substituting Eq. (20) in Eq. (19), the following equation can be obtained

$$\begin{cases} P_{\rm cr} = \frac{f_{\rm tk} b^2 h [bh + (\alpha \cos \theta - 1) A_{\rm sc}]}{b^2 h + 6\alpha A_{\rm sc} [R_1(\cos \theta - \cos \theta_0) + R_2(1 - \cos \gamma_0)]} \\ (\theta \le \theta_0) \\ P_{\rm cr} = \frac{f_{\rm tk} b^2 h [bh + (\alpha \cos \theta - 1) A_{\rm sc}]}{b^2 h + 6\alpha A_{\rm sc} R_2 [1 - \cos(\gamma_0 - \gamma)]} \\ (\gamma \le \gamma_0), \end{cases}$$
(21)

When  $\theta$  = 0, the cracking load was minimum, meaning that the first crack was most likely to occur in the mid-span section. Substituting  $\theta$  = 0 into Eq. (21), the equation for calculating the cracking load of an axially tensioned concrete member reinforced with the SCAHS can be obtained as Eq. (20). Considering the discrete nature of the concrete strength, a certain possibility also exists in the zone near

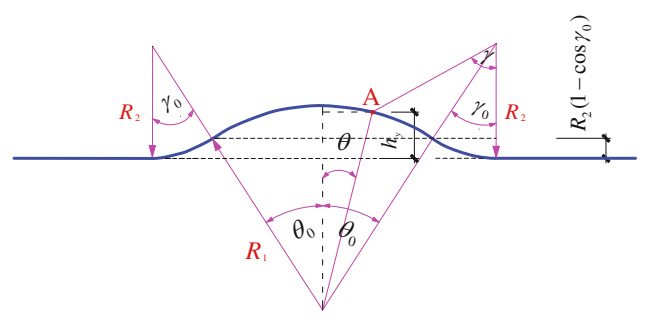


Figure 18: Sketch of height calculation at any point of the curved section.

the mid-span section. Due to the presence of additional bending moments, cracks should first appear in the inner concave side of the member.

$$P_{\rm cr} = \{ f_{\rm tk} b^2 h [bh + (\alpha - 1)A_{\rm s1}] \} / \{ b^2 h + 6\alpha A_{\rm s1} [R_{\rm l}(1 - \cos \theta_0) + R_2 (1 - \cos \gamma_0)] \}.$$
 (22)

### 4.2 Tensile analysis of concrete members reinforced with multiple SCAHSs

### 4.2.1 Additional bending moment and cracking load

When a member reinforced with multiple SCAHSs was subjected to axial tension, additional bending moments need to be superimposed. If the cross-sectional area of a single reinforcing bar was still  $A_{\rm sc}$ , the additional bending moment was

$$M_{\rm r} = \frac{n\alpha A_{\rm sc} P h_{\rm a}}{bh + n(\alpha - 1)A_{\rm sc}}.$$
 (23)

As can be seen from the above equation, the internal forces of members reinforced with multiple SCAHS can be directly replaced by  $nA_{\rm sc}$  instead of  $A_{\rm sc}$ . The effect of the additional bending moment of multiple SCAHSs increased in the crack load calculation. When calculating the maximum tensile stress from the additional bending moment of the SCAHSs, it should be based on the area of the converted section, setting the direction as around the coordinate axis z, i.e., the maximum concrete stress and cracking load calculation with the modulus of the converted flexural section  $W'_{0z}$  around the direction z instead of  $b^2h/6$ .

### 4.2.2 Force characteristics after cracking

Compared to the concrete member reinforced with a single SCAHS, cracks in concrete members reinforced with multiple SCAHSs started at the concave side of the SCAHSs and was rapidly confined as the cracks developed into the first SCAHS, with much smaller additional bending moment effects in the SCAHSs. The section can still be cracked through because the stress from the additional bending moment was still much less than the stress from the axial tension. Similarly, after cracking, there was a tendency for the SCAHSs at the crack to be taut. The stress after taut was basically the same as that of the member reinforced with straight steel bars, but the stress state in the uncracked range of the member was still small eccentric in tension.

### 5 Load bearing capacity limit state stress analysis and allowable crack widths

## 5.1 Load carrying capacity limit state stress analysis and load carrying capacity equations

The anti-arc point section  $(\theta = \theta_0)$  of SCAHS was the most dangerous section. In this section, when the member entered the damage phase, the reinforced part of the concave side of SCAHS yielded first due to the bending moment in the width direction of the section caused by SCAHS, and gradually developed toward the convex side; as the load increased, the stress entered the strengthening phase from the concave side of SCAHS to the convex side in turn. The tensile stress was greatest at the outermost edge of the concave side of SCAHS, which reached the ultimate strength first and the member reached the maximum load carrying capacity. As can be seen from Figure 13(b), when the internal forces carried by the section reached the ultimate strength from the yield strength, the deformation of the member increased insignificantly. Considering the ductility of the cross-section and following the yield strength of the reinforcement as the basis of engineering design, the bending moment borne by the tensile reinforcement was the ultimate bearing capacity of the cross-section when it was fully yielded, and the concrete at the edge of the compressed zone was considered to be crushed at this time. From the basic assumptions of calculating the normal section of the flexural member and the equivalence of the rectangular stress pattern, the following equations of the limit state can be obtained:

$$f_{\rm c}bx = f_{\rm v}A_{\rm s}\cos\theta_0,\tag{24}$$

$$M_{\rm u} = f_{\rm y} A_{\rm s} \cos \theta_0 \left| h_0 - \frac{x}{2} \right|.$$
 (25)

Bringing the parameters of A4 slab ( $f_{\rm c}$  = 28.65 MPa,  $f_{\rm y}$  = 497.8 MPa,  $A_{\rm s}$  = 471 mm<sup>2</sup>,  $\cos\theta_0$  = 0.946, b = 800 mm) into Eqs (21) and (22), it can be obtained that the ultimate load was 71.0 kN, which was close to the test result of 70 kN.

#### 5.2 Allowable crack widths

In hydraulic structures, curved arc reinforcement was used in mass concrete, which was a non-bar system structure, and the crack width needs to be calculated by finite element method. It was very inconvenient to model curved arc reinforcement when performing finite element analysis. If the allowable crack width of a SCAHSs reinforced concrete member can be converted to the crack width of a straight reinforcement, then hydraulic massive structures can be easily modeled by replacing the SCAHSs with the straight steel bars for finite element calculations.

In this article,  $\beta$  was used to represent the ratio of the measured maximum crack width of SCASBs reinforced concrete slabs to the measured maximum crack width of straight steel bars reinforced slabs.  $\gamma$  was equal to  $1/\beta$ . Table 9 shows  $\beta$ ,  $\chi$ , and  $w_{\text{max}}$  for SCAHSs reinforced concrete slabs with different sagittal heights. The effect of creep was not considered. The allowable crack width for SCAHSs reinforced concrete slabs under environment category I was 0.27 mm. For concrete slabs reinforced with SCAHSs of 650.0 mm vector span and 54.5 mm vector height, the range of  $\gamma$  was from 0.89 to 1.08, and  $\gamma$  = 0.89 can be safely adopted. For concrete slabs reinforced with SCAHSs of 500.0 mm vector span and 31.8 mm vector height, the range of  $\gamma$  was from 0.76 to 0.85, and  $\gamma$  = 0.76 can be safely adopted. In other words, when calculating SCAHSs reinforced concrete members according to straight steel bars reinforced concrete members, the allowable crack widths can be taken as 0.24 and 0.20 mm, respectively, and 0.2 mm for calculation convenience. The allowable crack width of SCAHSs reinforced concrete slabs under environment category II was 0.20 mm, and  $\gamma = 0.87$  can be safely adopted, i.e., the allowable crack width can be taken as 0.17 mm when calculating SCAHSs reinforced concrete members according to straight steel bars reinforced concrete members. The allowable crack width of SCAHSs reinforced concrete slabs under environment category was 0.17 mm. For slab concrete slabs

**Table 9:**  $\beta$ ,  $\chi$ , and  $w_{\rm max}$  for SCAHSs reinforced concrete slabs with different vector heights

Load (kN)	w <sub>max</sub> (mm)		or height 4.5 mm		r height 8 mm
		β	χ	β	χ
160	0.13	1.15	0.87	1.15	0.87
180	0.13	1.38	0.72	1.15	0.87
200	0.15	1.47	0.68	1.20	0.83
220	0.18	1.39	0.72	1.00	1.00
230	0.20	1.35	0.74	1.10	0.91
240	0.20	1.50	0.67	1.15	0.87
250	0.25	1.08	0.93	1.20	0.83
260	0.25	1.12	0.89	1.32	0.76
275	0.30	0.93	1.08	1.17	0.85

reinforced with SCAHSs of 650.0 mm vector span and 54.5 mm vector height, the range of  $\chi$  was from 0.68 to 0.72, and  $\chi$  = 0.68 can be safely adopted. For concrete slabs reinforced with SCAHSs of 500.0 mm vector span and 31.8 mm vector height, the range of  $\chi$  was from 0.83 to 1.00, and  $\chi$  = 0.83 can be safely adopted. In other words, when calculating SCAHSs reinforced concrete members according to straight steel bars reinforced concrete members, the allowable crack widths can be taken as 0.12 and 0.14 mm, respectively, and 0.12 mm for calculation convenience.

### 6 Conclusions

The damage process and mechanism of SCAHSs reinforced concrete slabs were analyzed by testing the flexural performance of straight steel bars and SCAHSs reinforced concrete slabs. The characteristic load, deflection, crack spacing, and crack width were calculated. Combined with the test results, the synergistic tensile work of SCAHS and concrete was analyzed. The equations for the load carrying capacity and allowable crack width of the SCAHSs were given. The main conclusions can be obtained as follows.

- 1) After replacing the straight steel bars in concrete slabs with SCAHSs, the cracking load of the concrete slabs did not change much, and the crack width of the concrete slabs increased, with the maximum crack width at the bottom of the concrete slabs increasing by a factor of 1.2–1.4. As the rise-span ratio of SCAHSs increased, the flexural stiffness of SCAHSs reinforced concrete slab decreased slightly, but the deflection increased.
- When the concrete slab reinforced with the SCAHS was subjected to bending, the most dangerous cross-section was the section at the anti-arc point of the SCAHS, with maximum crack width and damage occurring near the anti-arc point of the SCAHS. The slabs reinforced with the SCAHSs with small width, strong shear, and weakly bending performed bending and torsional damage pattern, indicating that the horizontal component stresses generated by the curved reinforcement had a greater impact in the later loading stage. The reinforcement entered the strengthening phase when the concrete slab was damaged.
- 3) In hydraulic massive structures, the allowable crack widths of SCAHSs reinforced concrete members was converted to those of concrete member reinforced with straight steel bars to facilitate modeling. The allowable crack widths of concrete member reinforced with SCAHSs under environment categories I, II, and III were 0.20, 0.17, and 0.12 mm, respectively.

4) In the calculation of normal section load capacity, SCAHSs reinforced concrete slabs can be regarded as straight steel bars reinforced concrete slabs with a longitudinal reinforcement area of  $A_s \cos \theta_0$ , which was similar to the test results. It was recommended to use it as the basis for load-bearing design, where  $\theta_0$  was half of the large arc angle of the SCAHS.

**Acknowledgments:** The authors acknowledge the support by China Scholarship Council; the Natural Science Research Project of Jiangsu Province Colleges and Universities (21KJD560002), China; Suqian Natural Science Foundation Project (K202012), China; Project funded by the research and innovation team of engineering structure seismic tech-nology of Sugian University in 2020, China; Sugian City Guiding Science and Technology Plan Project (Z2020137), China; Research and Innovation Team Project of Sugian College (2021TD04), China; the Fifth Provincial Research Funding Project of "333 High-level Talent Training" in 2020 (BRA2020241), China; The Youth Fund Project of Sugian College (2023XQNA03); Natural science research project of Jiangsu Province higher education institutions, China (23KJA560007); and Jiangsu Civil Architecture Society project, China ((2023) No. 4 Item 9).

**Funding information:** This research has been supported by China Scholarship Council; the Natural Science Research Project of Jiangsu Province Colleges and Universities (21KJD560002), China; Sugian Natural Science Foundation Project (K202012), China; Project funded by the research and innovation team of engineering structure seismic technology of Sugian University in 2020, China; Sugian City Guiding Science and Technology Plan Project (Z2020137), China; Research and Innovation Team Project of Sugian College (2021TD04), China; the Fifth Provincial Research Funding Project of "333 High-level Talent Training" in 2020 (BRA2020241), China; The Youth Fund Project of Sugian College (2023XQNA03); Natural science research project of Jiangsu Province higher education institutions, China (23KJA560007); and Jiangsu Civil Architecture Society project, China ((2023) No. 4 Item 9).

**Author contributions:** All authors have accepted responsibility for the entire content of this manuscript and approved its submission.

**Conflict of interest:** The authors state no conflict of interest.

**Data availability statement:** All data generated or analyzed during this study are included in this published article.

### References

- [1] Yang, B. G., P. He, G. Y. Peng, and L. Tong. Temperature-stress coupling mechanism analysis of one-time pouring mass concrete. *Thermal Science*, Vol. 23, 2019, p. 231.
- [2] Lu, X. C., B. F. Chen, B. Tian, Y. Li, C. Lv, and B. Xiong. A new method for hydraulic mass concrete temperature control: Design and experiment. *Construction and Building Materials*, Vol. 302, 2021, id. 124167.
- [3] Xin, J. D., Y. Liu, G. X. Zhang, Z. Wang, N. Yang, Y. Qiao, et al. Comparison of thermal cracking potential evaluation criteria for mass concrete structures. *Materials and Structures*, Vol. 54, No. 6, 2021, pp. 243.1–243.15.
- [4] Li, S. H., Z. Y. Wang, L. Y. Yang, X. M. Deng, and Y. Li. Study on the causes and prevention measures of cracks in high crushed concrete dams. *Water Resources and Hydropower Technology*, Vol. 48, No. 1, 2017, pp. 98–102.
- [5] Chen, P. P. and G. Zhang. Study on the prevention measures and causes of cracks in arch crests of galleries in high concrete dams. Advanced Materials Research, Vol. 3149, 2014, pp. 919–921.
- [6] Woo, H. M., C. Y. Kim, and J. H. Yeon. Heat of hydration and mechanical properties of mass concrete with high-volume GGBFS replacements. *Journal of Thermal Analysis and Calorimetry*, Vol. 132, No. 1, 2018, pp. 599–609.
- [7] Liu, X. H., C. B. Zhou, X. L. Chang, and X. Zhou. Simulation of temperature crack expansion process in mass concrete. *Geotechnics*, Vol. 8, 2010, pp. 2665–2676.
- [8] Jiang, X. P., S. L. Wang, S. X. Duan, and Y. Sun. Analysis of the mechanism of temperature cracks in super-volume concrete and new countermeasures for crack control. *Concrete*, Vol. 12, 2007, pp. 98–102.
- [9] Gao, F. L. and Y. W. Fang. Temperature cracks controlling technology for the mass concrete in solid sections of lower pylon column. *Applied Mechanics and Materials*, Vol. 467, 2013, pp. 262–269.
- [10] Yan, L., Y. D. Wen, and W. Bo. The finite element analysis of temperature cracking propagation process of pouring mass concrete. *Applied Mechanics and Materials*, Vol. 302, 2013, pp. 499–501.
- [11] Shi, W. and J. P. Hou. Temperature control performance of bulk concrete with phase change temperature control under different conditions. *Journal of Construction Materials*, Vol. 16, No. 6, 2013, pp. 1063–1066.
- [12] Ma, Y. Z. Study on the contact state of reinforcement and transverse joints in the bottom slab of the upper gatehead of Tingzikou. *Master's Thesis*. Hohai University, Nanjing, China, 2014.
- [13] MOHURD (Ministry of Housing and Urban-Rural Development of the People's Republic of China). *Code for design of concrete structures (GB50010-2010)*, China Architecture & Building Press, Beijing, 2015.
- [14] Power Industry Standards of the People's Republic of China. *Design specification for hydraulic concrete structures (DL/T5057-2009)*, China Electric Power Press, Beijing, 2009.
- [15] Standard of Mistry of Water Resources of the People Republic of China. Design code for hydraulic concrete structures (SL191-2008), China Water & Power Press, Beijing, 2008.